Geoderma 361 (2020) 114017

Contents lists available at ScienceDirect

Geoderma

journal homepage: www.elsevier.com/locate/geoderma

The application of rapid handheld FTIR petroleum hydrocarbon-contaminant measurement with transport models for site assessment: A case study

Liang Wang[a,b,*], Ying Cheng[a,b], Dane Lamb[a,b], Ravi Naidu[a,b]

[a] Global Centre for Environmental Risk Assessment, Faculty of Science and Information Technology, The University of Newcastle, Callaghan, NSW 2308, Australia
[b] CRC for Contamination Assessment and Remediation of Environment, ATC Building, Callaghan, NSW 2308, Australia

ARTICLE INFO

Handling Editor: Alex McBratney

Keywords:
Petroleum hydrocarbons (PHs)
Fourier transform infrared spectroscopy (FTIR)
Hydrus modelling
Revised Universal Soil Loss Equation (RUSLE)
ArcGIS mapping

ABSTRACT

Conventional contaminated site assessment requires sophisticated sampling and laboratory analyses, which are costly and time consuming. There is a trend for soil analyses to shift from complex laboratory procedures to rapid, simple and non-destructive spectroscopic methods that can be used in the field. Handheld Fourier Transform Infrared (FTIR) spectroscopy has the advantage of providing information for rapid *in situ* site characterisation. To apply the infrared (IR) spectral application for petroleum hydrocarbon (PH) contamination site investigation, the coherent bands at locations from 3000 to 2800 cm^{-1} represent carbon (C) – hydrogen (H) bonding for long-chain alkanes due to –C–H stretching vibrations. The areas of the coherent bands at these locations can be used to quantify the total petroleum hydrocarbon (TPH) concentrations in soils. With additional spectral data from IR spectroscopy there is potential for predicting soil texture and water content, which are the basic inputs for modelling the migration of PH at contaminated sites. This study demonstrates the innovative coupling of spectral analytical models and a handheld FTIR instrument, with a soil erosion model, the Revised Universal Soil Loss Equation (RUSLE), and the Hydrus hydrological model. The integration of these models were used to investigate the potential downstream water and groundwater contamination risks from the migration of PH at a PH-contaminated site.

1. Introduction

In conventional contaminated site characterisation, soil sampling and sample transportation from sites are cost prohibitive and time consuming. The application of portable and affordable field equipment provides a rapid and cost effective solution to alternate the complex laboratory analyses. Handheld Fourier Transform Infrared (FTIR) spectroscopy has advantages of providing instant results, ease of use and non-destructive measurements, thus allowing rapid *in situ* site characterisation.

The use of infrared spectroscopy for soil analysis has been widely studied. Soriano-Disla et al. (2014) summarised the current performance of mid-infrared (IR) reflectance spectroscopy for prediction of soil physical, chemical and biological properties. Table 1 below shows the calibration range for selected minerals commonly found in soils. Quartz is the most common constituent of sand and can be used to estimate the sand content in soils. As a major natural clay material, kaolinite is abundant in Australian soils, especially in warm and moist environments. Quantitative prediction of quartz and kaolinite can approximate sand and clay, and can thus act as a proxy for soil texture. In addition, coherent bands located at 3000–2800 cm^{-1} provide evidence of carbon (C) – hydrogen (H) bonding in long-chain alkanes due to –C–H stretching vibrations (Wang et al., 2019). The areas of these coherent bands can be used to quantify the total petroleum hydrocarbon (TPH) amount in a petroleum hydrocarbon (PH) – contaminated soil. Therefore, the information obtained from IR spectroscopy has the potential to provide basic inputs for environmental modelling. For example, when an oil spillage or leakage occurs on land, multiphase sequestration and distribution of PHs in porous soil media are affected by the hydraulic and physical properties of the soil as well as its hydration status (Nathwani and Philips, 1997; Greene-Kelly, 1954a,b; German and Harding, 1969; Olejnik et al., 1974; Mercer and Cohen, 1990; Williams et al., 2003). Mathematical models can be applied for estimating the potential for downstream surface water and groundwater

* Corresponding author at: Global Centre for Environmental Risk Assessment, Faculty of Science and Information Technology, The University of Newcastle, Callaghan, NSW 2308, Australia.
E-mail address: liang.wang@newcastle.edu.au (L. Wang).

https://doi.org/10.1016/j.geoderma.2019.114017
Received 14 July 2019; Received in revised form 2 October 2019; Accepted 16 October 2019
Available online 16 November 2019
0016-7061/

Table 1
FTIR calibration range frequencies for select soil minerals.

Minerals	Quartz	Kaolinite	Smectite	Illite
Calibration frequency range (cm^{-1})	1100–1000	3690–3620	3400–3300	3400–3300

contamination risks from the migration and transport of PH from contaminated sites.

The Hydrus model can be applied to estimate the downward movement of PH in soils with infiltrating water and for assessing the risk of groundwater pollution (Ma et al., 2014; Pan et al., 2013). In the Hydrus model, parameters of water retention and hydraulic conductivity can be estimated using pedotransfer functions, such as the van Genuchten–Mualem and Brooks-Corey model (Van Genuchten and Nielsen, 1985; Simunek et al., 2008). To apply these pedotransfer functions, users are required to provide the information of soil texture, sand %, silt % and clay %. Transport of PHs can then be modelled using Hydrus solute transport models. Key determinants for such a model include soil organic matter (SOM) and soil bulk density (BD). Hence, basic soil analyses are essential for the determination of parameters used in Hydrus model.

Soil erosion by water is one of the most important land degradation problems and a critical environmental hazard worldwide (Devatha et al., 2015). Erosion models, such as the Revised Universal Soil Loss Equation (RUSLE), can be applied to estimate the annual soil loss from a contaminated site in runoff water and suspended sediment (Renard et al., 1997; Wischmeier and Smith, 1978). Soil is a highly reactive media that preferentially adsorbs molecules and particles from solution or suspension (Yong et al., 1992). At a PH contaminated site, less volatile PHs will diffuse as oil or non-aqueous liquid (NAPLs) forms through the porous medium, and be trapped in pores or be adsorbed at mineral and organic matter surfaces. If the concentrations of PH in the surface soil are known, it should be possible to indirectly estimate annual losses of PH transported by surface runoff and subsequent downstream contamination associated with transported sediment and NAPLs.

In this study, our aim is to demonstrate, in principle, the coupling of data acquired by a handheld FTIR with online publicly available soil and meteorology information for estimating the potential risk of PH downstream transport to water bodies or to groundwater.

2. Materials and methods

2.1. Study area

A PH-contaminated site, located in the Pilbara region, Western Australia (Australia), was used as a case study. This site is a field workshop used for the maintenance and refuelling of heavy mining machinery. Diesel and lubricant oils are the main PH contaminants in the study area and stored on-site. Historically, spills and leaks have occurred during maintenance.

2.2. Handheld FTIR

For the FTIR measurements the surface soil (0–5 cm) from locations within the affected mine site were scanned directly in triplicate with a handheld FTIR (Agilent 4300). A coarse silver plate (99.99% Agilent) was applied as the background reference for the instrument calibration. To minimize the noise in spectral data, 32 'sample' scans and 64 'background'/'silver plate' scans were included in the infrared 4000–600 cm^{-1} region, at a scanning velocity of 2.5 KHz. 'Sample' scan was used to measure a soil sample with 32 times and average the spectral results. 'Background' scan was used to measure the reference silver plate for calibrating the instrument. The background calibration was done before sample measurements. All measurements of soil samples were made in diffuse reflectance infrared spectroscopy (DRIFTS) mode, and sampled non-destructively. There are several levels of spectral resolution: from 8 to 2 cm^{-1}. The lower the number of the spectral resolution, the higher resolution that can be achieved. However, high resolution would take a considerable amount of time for a scan and to obtain spectral data for computational analysis. An 8 cm^{-1} resolution was selected for this study as it has appropriate sensitivity and is practical for reduced sampling times and rapid screening for field related applications. By setting the resolution at 8 cm^{-1}, one measurement with 32 scans could be completed within thirty seconds. The infrared spectral data were obtained using Agilent Microlab PC software (Agilent). Using the Resolutions Pro FTIR software, the spectral data were saved in comma separated value (CSV) format, which is editable using Excel 2013. MATLAB R2016b was applied for method implementation, data processing and analysis. The infrared spectral data were processed by our in-house developed baseline correction method (Wang et al., 2019).

2.3. IR spectroscopy

According to our previous study (Wang et al., 2019), the coherent bands located at 3000 to 2800 cm^{-1}, represent carbon-hydrogen bonding of long-chain alkanes due to –C–H stretching vibrations. After background correction (Wang et al., 2015), the areas of these coherent bands were used to quantify the PH concentration in a soil sample. Calibration curves for the major soil constituents including quartz, kaolinite, humic acid (Sigma) was obtained using potassium bromide (KBr) discs (Nathwani and Philips, 1997). The IR spectra of the calibration standards are shown in Fig. 1. Quartz could be calibrated at 1080 cm^{-1} based on its Si-O stretching vibration (Soriano-Disla et al., 2014). Additionally, a secondary characteristic peak was observed at 804.5 cm^{-1}, indicating that these Si–O bending vibrations can also be applied for calibration. Kaolinite calibration can utilise the strong O–H stretching vibration presenting as the doublets at 3690–3620 cm^{-1}. The calibration could also consider the Si–O stretching at 1114 cm^{-1} or the Al–OH vibration at 959 cm^{-1}. However, these two IR bands are adjacent to the Si–O stretching vibration of quartz 1080 and 804.5 cm^{-1}. If these stretching bands were selected for calibration, there would be large interference without separation of quartz and kaolinite band when they occur simultaneously in a soil sample, which is commonly the case. For SOM, which is largely composed of humic substances, there was no single characteristic IR band that can be applied for quantitative analysis. Based on Greene-Kelley (Wang et al., 2019), alkyl groups were determined at 2930–2850 cm^{-1}, protein amide at 1670–1530 cm^{-1}, 1720 cm^{-1} for carboxylic acid, and 1600–1570 cm^{-1} for aromatic groups.

2.4. PH extraction and gas chromatography (GC)-flame ionization detector (FID)

In order to validate the FTIR method, the PH content of the soil samples used for FTIR study were also determined by GC-FID. The same soil samples were collected using 150 mL glass sampling jars for GC-FID analysis. PHs were extracted from each soil sample using a Dionex ASE 350 accelerated solvent extractor system (Thermo Fisher Scientific). This system uses organic and aqueous liquid solvents at elevated temperatures and pressure to increase the efficiency of extraction. Subsamples (0.5 g) of each soil sample were mixed with diatomaceous earth and loaded into the extracting cell. The oven temperature was set at 100 degree Celsius (°C) and pressure at 103.4 bar for the extraction cycle. PHs were extracted in 5 mL hexane for 5 min with a 60% rinse volume. After six extraction cycles the extracted solvents with a total volume of 30 mL each, were evaporated by nitrogen. Then 6 mL of hexane was added to the extractions to concentrate the samples. Then 1 mL of each solvent was collected into a 2 mL GC vial. GC data were collected using an Agilent 7890B GC system, with a HT-5 column of 12 m length by 220 μm inner diameter with 0.1 μm of film thickness.

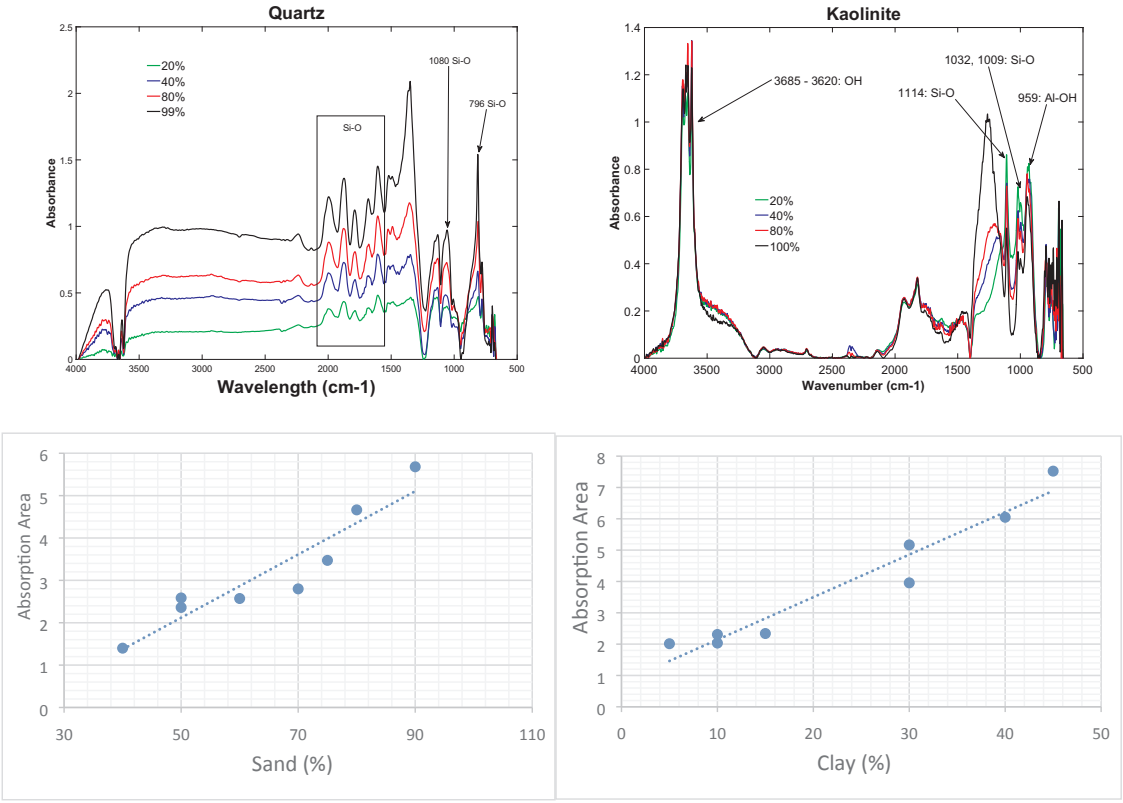

Fig. 1. FTIR calibration of minerals at varying content.

The column pressure was 0.76 bar with 22 mL/min flow rate. A front splitless inlet was applied to inject the sample into the GC column with helium as the carrier gas, and the pressure and temperature were set at 0.76 bar and 275 °C, respectively. A sample volume of 1 µL of was injected into the GC-FID. The whole GC programme sequence included a 35 min run time and 1 min post-run time. The GC column temperature started at 30 °C and held for 1 min, and then increased to 320 °C at increments of 10 °C/min, then held for 5 min. The GC oven maximum temperature was set as 340 °C. The temperature of FID detector was set at 320 °C with 40 mL/min fuel flow rate.

2.5. Soil mechanical analysis

To compare the determination method of FTIR, soil texture information for each soil sample was analysed using the micro-pipette method (Miller and Miller, 1987). Each soil sample (4 g) was added to 50 mL screw cap tube containing 40 mL of the dispersing solution made up of dilute sodium hexametaphosphate (Sigma-Aldrich) and sodium hydroxide (Sigma-Aldrich) (Kulikov, 2017). After shaking the tubes overnight and additional two hour settlement, 2.5 mL of suspension at 2.5 cm depth from each sample was extracted using a 5 mL pipette and dried overnight at 105 °C. The weight of the extracted suspension was used to calculate the clay content. For each sample, the remaining solution in the tubes was transferred to 53 µm sieve, and the > 53 µm fraction, remaining on the sieve was collected and dried in a 105 °C overnight. The weight of this fraction was used to calculate the sand content.

2.6. Hydrus

Hydrus-1D (PC-Progress) was applied to estimate the downward movement of PH in soils with infiltrating water and for assessing the risk of groundwater pollution (Ma et al., 2014; Pan et al., 2013). For the hydraulic model, van Genuchten-Mualem was applied in this study (Simunek et al., 2008). The basic input to the hydraulic model included: soil texture (% sand, % clay and %silt), SOM, soil BD and meteorological data (temperatures and rain precipitations). Soil texture data was obtained using IR spectroscopy. The soil BD and the SOM of the soil samples of the case study area were based on the online database of Soil and Landscape Grid of Australia. Weather data, averaged from 2009 to 2018, was obtained from the local weather station in Pilbara, Western Australia. For the water flow boundary conditions (BCs), the upper BC was set to use the precipitation using the meteorological data from the weather station, and the 'free drainage' was selected as the lower BC (Simunek et al., 2008). Heat transport was also applied in the application. The amplitude of the temperature fluctuation was determined based on the meteorological data from the weather station (Simunek et al., 2008).

For the equilibrium solute transport model, the 'Crank-Nicholson' model was used as the time weighted scheme, and the 'Galerkin Finite Elements' model was selected as the space weighting scheme. The mass unit was milligram per kilogram or ppm. The stability criterion was set to 2. The dispersivity was set to 0.1 and the dimensionless fraction, 'Frac', of adsorption sites, was set to 1 for the equilibrium transport. The immobile water content was equal to 0 as the physical non-equilibrium option was not considered. The molecular diffusion coefficient in free water and soil air were set to zero.

2.7. Rusle

Rusle allows prediction of annual soil loss based on six main factors (Ganasri and Ramesh, 2016) as follows:

$$A = R * K * (LS) * C * P \quad (1)$$

where:

- A is computed spatial average soil loss and temporal average soil loss (g/m^2) per year;

- R is rainfall and runoff erosivity;
- K represents the soil erodibility factor is an indicator of how susceptible the soil is to the erosive action of precipitation – drop splash and surface runoff, and is dependent on the physical characteristics of soils (Römkens and Poesen, 1987; Kulikov, 2017).
- L is the slope length factor and S is the slope steepness factor
- C represents the effects of surface cover and roughness on soil erosion and
- P is an expression of the effects of specific conservation practice in the soil such as contouring, strip cropping, terracing and subsurface drainage.

The R factor reflects the effects of rainfall intensity on soil erosion. According to Kassam et al. (1992), the relationships between the Mean Annual Rainfall (MAR) and Rainfall Erosivity (R) can be expressed as Eq. (1):

$$When\ MAR\ \leq 900\,\text{mm} : R = 0.21 \times MAR + 97.75 \quad (1.1)$$

$$When\ MAR\ \geq 900\,\text{mm} : R = 0.61 \times MAR - 304.8 \quad (1.2)$$

The K factor was estimated using the Textural Triangle monograph developed by Austin Erickson to determine most of the soil erodibility (K) factors (Rogers et al., 2002). The L and S factors reflect the influence of terrain on soil erosion, which has the greatest impact on modelling soil loss. Both the L and S factors were calculated using the spatial analysis function in ArcGIS, with the digital elevation model (DEM) obtained from National Elevation Data Framework, Geoscience Australia (Mitasova et al., 1996). The L factor was calculated using the flow direction and flow accumulation (flowacc) functions and the S factor was calculated using the slope analysis function. The final LS result can be expressed using as

$$LS = 1.4 \times \left(\frac{[flowacc] * resolution}{22.1}\right)^{0.4} \times \left(\frac{Sin(slope) * 0.017]}{0.09}\right)^{1.4} \quad (2)$$

where:

- L is the slope length factor and S is the slope steepness factor
- Flowacc is the raster result of the calculation of the flow accumulation and direction functions using the DEM data;
- Resolution is the resolution of the raster Flowacc;
- Slope is the steepness raster result calculated using the slope function.

Factors C and P are the mitigation effects of the crop or vegetation cover on soil erosion, and it varies between 0 and 1 (Ali and Hagos, 2016). The value approaching 0 indicates good conservation practice and the value approaching 1 indicates poor conservation practice. In this work, the maximum likelihood classification method was used to determine the C and P factors in ArcGIS.

3. Result and discussion

3.1. Handheld FTIR results

The area under the curve (bands), at wavenumber 3000–2800 cm^{-1}, of each soil sample measured by handheld FTIR were compared with the values determined by the GC-FID conventional laboratory method. The linear regression model was applied to relate the area to the concentration of PH. Fig. 2a shows the comparison between the FTIR and the TPH results in the soil samples determined by GC-FID. Over the concentration range from 1 to 50 g of TPH in 1 kg of soil, g/kg (‰ w/w), there was a close linear relationship between the FTIR and GC-FID results. The slope coefficient, R^2 value were close to 0.95. This suggests that FTIR results accounted for 95% of the variance in GC-FID values. According to our sample analytical results, the linear range of handheld FTIR for PH measurement was from 0.5 to 50 g/kg. Based on the measurement results, the distribution of PH at the contaminated site (Kriging interpolation, ArcGIS) is displayed in Fig. 2. At the site, the hotspots containing high levels of PHs were located at the northern end. In the northern end, concentrations as high as 112 g/kg were observed, which was associated with waste storage.

For quantitative analysis of soil properties using infrared spectroscopy, it is apparent that the Si–O peak at 796 cm^{-1} can be used for quantitative analyses of quartz. The peak from 3700 to 3600 cm^{-1} can be used for quantitative analysis of kaolinite. The correlations between the IR absorption band area integration and known percentage in the mixtures were 0.94 and 0.87, for kaolinite and quartz, respectively. After determining the proportions of sand and clay, silt was obtained by calculating the difference. Based on the measurement of nineteen soil samples using FTIR, the Kriging interpolated soil texture results of the contaminated site were mapped, as illustrated in Fig. 3. Sand content varied from 36% to 75%, silt from 22% to 48% and clay from 6% to 16%. Comparing the FTIR measurement results against the micro-pipette method, the mean of relative errors for sand, silt and clay were 0.89, 0.87 and 0.91 respectively.

For SOM content quantification, numerous quartz and kaolinite peaks below 2000 cm^{-1} almost completely overlap peaks from SOM. However, it was observed that there were minor bands that appear to be noise around the 3500 cm^{-1} and 1720–1630 cm^{-1} regions, which can be considered as humic acid substances. In addition, minor peaks at the region around 2930 cm^{-1} could be observed when humic acid content was more than 10%, which could be applied for humic acid calibration in soil that is not contaminated with PH. However, this region only represents one functional group of humic acid, and the region overlaps with bands used for PH determination. Hence, it was difficult to use IR spectroscopy to determine organic matter content in PH contaminated soils and vice versa. Furthermore, PH pollution increases SOM content, which is attributed to the presence of NAPL, creating anaerobic conditions leading to the death of most aerobic microorganisms (Olejnik et al., 1974). The dead organisms contribute to SOM (Nudelman et al., 2002). Hydrocarbon-degrading bacteria can be present in low numbers in unpolluted environments and reach high densities after coming into contact with released petroleum compounds due to energy-rich carbon-hydrogen bonds (Head et al., 2003). In our application, it was difficult to apply IR spectroscopy to quantify SOM.

3.2. Hydrus model

Inputting the values of soil texture, Hydrus applied an artificial neural network (ANN) to predict the relative input values of the soil hydraulic parameters, including residual water content, saturated water content and hydraulic conductivity (K_{sat}), air entry suction 'Alpha' and pore-size distribution 'n', for the hydraulic models (Simunek et al., 2008). Fig. 3 shows the soil K_{sat} distribution using kriging interpolation.

According to the meteorological data obtained from the local weather station, it can be observed that the wet season extends from December to March accounting for one-third of the annual total, which was 31 cm (ten-year average) (Fig. 4a and b). The mean annual temperature was 21.3 °C. Winter is from June to August, and the driest period is from August to October. Using the soil sample from the northeast corner as a demonstration, the percentage of sand, silt and clay were 74%, 14% and 12%, respectively. By using the ANN algorithm from Hydrus, the predicted residual and saturated water content were 4.8% and 38%, respectively. K_{sat} was 48.5 and Alpha was 0.035 cm^{-1}. Fig. 4c and d shows the soil water content (Θ) and temperature variations of the modelled three year period in three different depths. There were three observation depths at the surface, 25 cm and 50 cm. It was observed that the deeper soil was less susceptible to changes in temperature and Θ.

For the solute transport model, adsorption–desorption distribution (K_d) and soil BD are two important factors that significantly affect the solute transport by using Crank-Nicholson and Galerkin Finite Elements

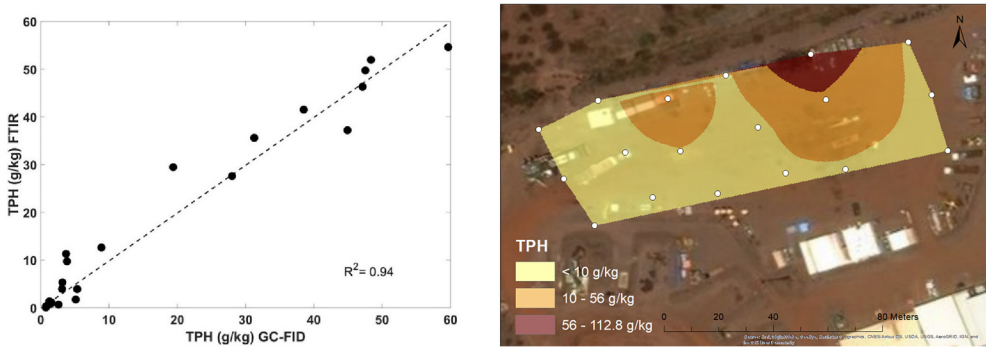

Fig. 2. Comparison of PH from FTIR and GC-FID, and (right) spatial distributions of PH determined from the case site.

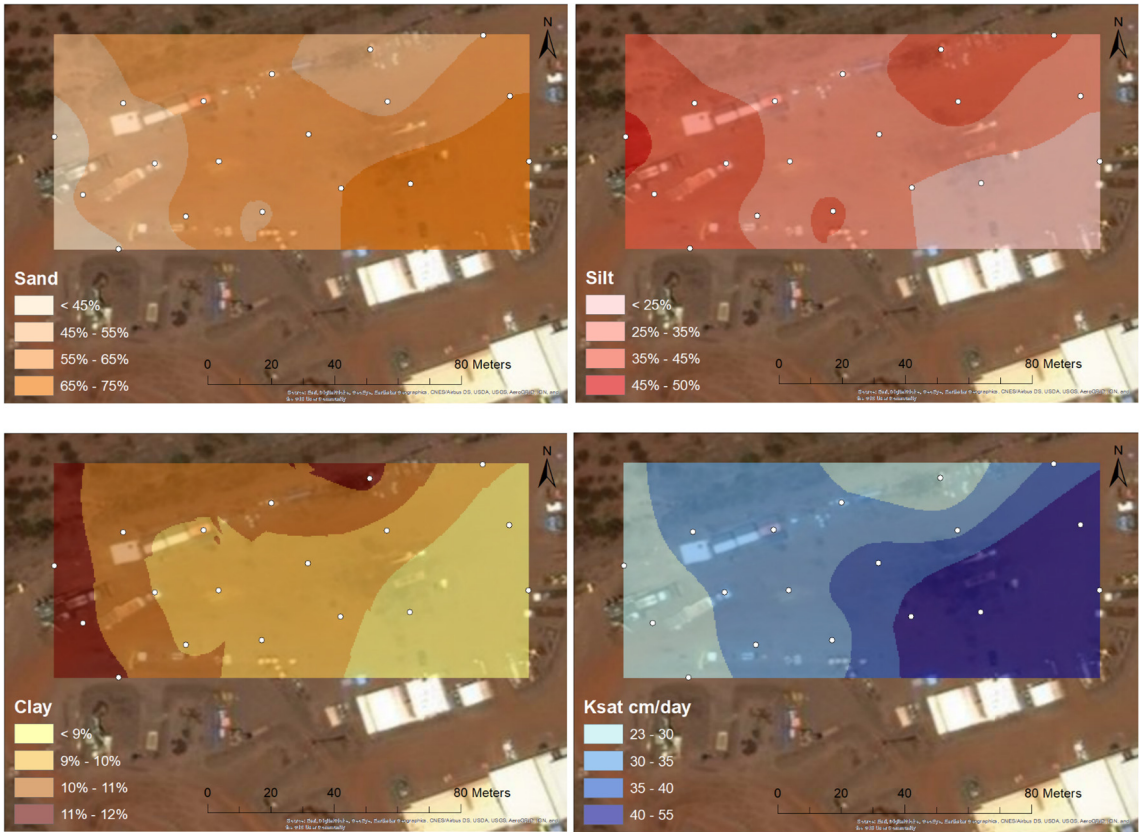

Fig. 3. The soil textures (sand%, silt% and clay%) and related hydraulic conductivities (Ksat) of the soil samples.

scheme in Hydrus. Soils with greater SOM content adsorbed more PHs than those with smaller concentrations (Benka-Cooker and Ekundayo, 1995; Uzoije and Agunwamba, 2011). SOM dominates overall sorption of PHs when it is present at greater than 1% (Benka-Cooker and Ekundayo, 1995). At low concentrations of organic matter the adsorption capacity of clays and other minerals may become important, especially under arid conditions (Benka-Cooker and Ekundayo, 1995). The value for K_d varies greatly because of variation in SOM. It is useful to express the K_d, as the soil organic carbon-water partitioning coefficient (K_{OC}) multiplied by the mass fraction of soil organic carbon content (f_{OC}). K_{OC} is frequently estimated based on the octanol-water partition coefficient (K_{OW}) (Karickhoff, 1981). Sadler and Connell (Sadler and Connell, 2003) listed the K_{OC} values for both aliphatic fractions and aromatic PH fractions. Since the PH-contaminated soil samples were dominated by diesel's PH aliphatic fraction, C16–C35, log K_{OC} was set at 8.8 (Sadler and Connell, 2003). The soil BD and SOM of the soil samples of the case study area were 1.4 g/cm^3 and 0.5%, respectively, based on the online database of Soil and Landscape Grid of Australia. Hence, the K_d was estimated as 33.2. The adsorption isotherm coefficient and exponent were set to 0 and 1, respectively. Other constants required for the model, including 'Henry' and 'Sink water/gas', were set to 0.

To study PH infiltration using the Hydrus model, we also simulated two soil spill scenarios. In both scenarios, we applied the PH concentrations and soil hydraulic properties included in Figs. 2 and 3, respectively. The first simulation scenario was a one-off diesel spill to the top of the uncontaminated soil. For the second simulation scenario diesel was assumed to have leaked constantly from an oil storage tank for over ten years. Other parameters remained at the same values, assuming no natural attenuation and biodegradation. The annual rainfall and temperature data (Fig. 4) were applied repeatedly for ten-year simulation. By observation, PHs with 500 mg/kg, reached similar depths at the same sample locations, over the ten-year simulation for both of the scenarios. The results are displayed in Fig. 5.

Increasing soil organic matter will increase PH K_d. In our simulation for instance, the initial deepest infiltration was approx. 30 cm. At

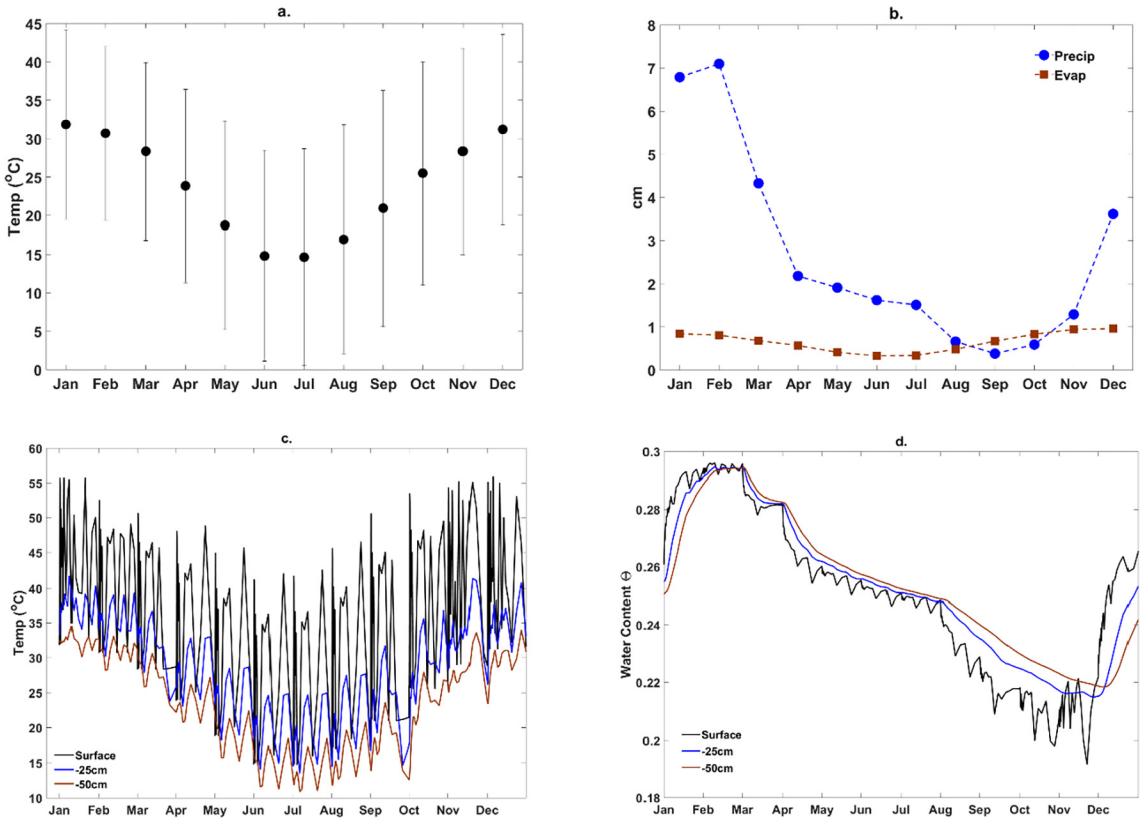

Fig. 4. (a) The monthly temperature averaged from 2009 to 2018. (b) Monthly rainfall and evaporation averaged from 2009 to 2018. (c) The simulated soil temperature (°C) at three different depth of soil. (d) The simulated water content (Θ) at three different depth of soil.

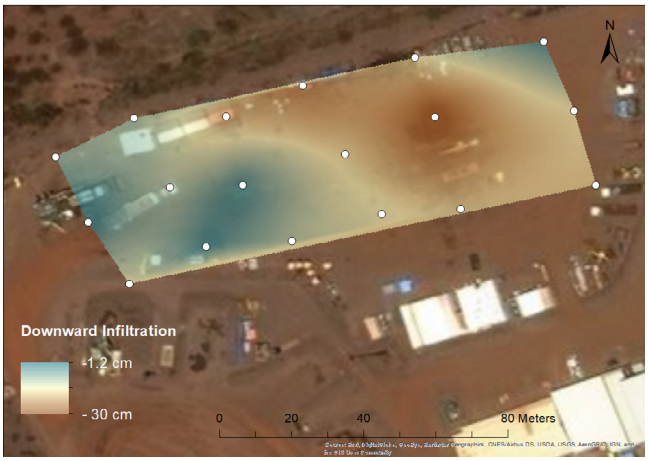

Fig. 5. Ten year downward infiltration depth for PH at 500 mg/kg.

30 cm, the PH concentration was lower than 0.5 mg/kg, which is the detection limit for most of the instruments (Sadler and Connell, 2003). If the SOM was increased to 1%, K_d would double to 66.2. If the other parameters had the same values the PHs could not infiltrate as far deep as 20 cm over the simulated ten years. If biodegradation and natural attenuation are considered by setting the first deviation of 'SinkWater', 'SinkSolid' and 'SinkGas' to 0.001, the PHs could infiltrate as deep as 10 cm in the same period. Therefore, there is low risk of groundwater pollution in the foreseeable future. The groundwater at the study area was more than 5 m below surface. Furthermore, PH pollution alters both the chemical and physical properties of soil by aggregating soil particles in plaques, lowering porosity, increasing resistance to penetration, and thus causing an increase of soil BD (Uzoije and Agunwamba, 2011). On the other hand, increasing the soil BD from 1.4 to 1.6 g/cm^3, the infiltration depth of PH would decrease from 30 cm to 24 cm over the simulated ten year period. Hence PH infiltration could be lower than the simulation results if all the factors, including the variation of SOM, BD, and biodegradation, were considered.

3.3. RUSLE model

According to the ten-year average rainfall data shown in Fig. 4, the MAR of the mine site was 319.8 mm, and R was 164.91 MJ*mm/ha*h*yr. Accordingly, with the soil texture data shown in Fig. 3, the K factor was estimated using the Textural Triangle monograph. The annual soil loss caused by surface runoff was estimated from the erosion model (Fig. 6). The less volatile PHs tend to become trapped in soil pores or adsorbed at mineral and organic matter surfaces. During erosion, the PHs trapped or adsorbed in the soil media could be carried by surface runoff, and therefore, potentially contaminate downstream water bodies. In this study, we calculated PH loss based on the FTIR estimated PH concentration in the surface soil samples (Fig. 2). The results for PH loss in the site are shown in Fig. 7. It is clear that the area with most PH loss by erosion coincided with hotspot, with annual losses around 143 g/m^2. The amount of PHs that could be carried by surface runoff and stay in sediment or flow with water as NAPLs to downstream areas were calculated using sediment yield models. However, as shown by the LS factor plot in Fig. 6, the site is located in a depression and all the water flow accumulations are mostly towards the site. Hence the risk of downstream contamination is low, and soil infiltration and groundwater contamination were considered as the more likely risk of environmental pollution.

4. Conclusion

A hand-held FTIR has the advantage of providing rapid *in situ* PH contaminated site characterisation. After proper calibrations this non-

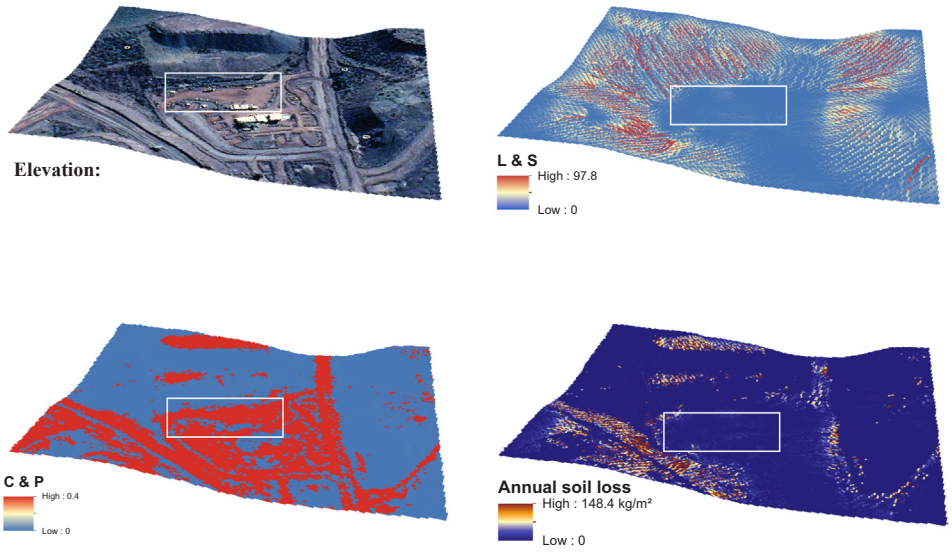

Fig. 6. RUSLE erosion model for the Ponderosa site.

Fig. 7. Mapping of TPH annual loss by erosion at the case study site.

destructive spectroscopic method can determine both PH and soil texture, which can then be applied as inputs to an transport models (RUSLE, Hydrus) to investigate the potential downstream and groundwater contamination risks from migration of PH. The erosion model RUSLE was applied to calculate the annual soil loss for the entire site. Based on the concentrations of PH in the surface soil sample, we can indirectly estimate the PH annual losses which can be carried by surface runoff and contaminate downstream environments. The Hydrus model was applied to investigate the downward soil transport as infiltration to assess the risk to groundwater. Based on our modelling, the PHs could reach 30 cm depth within our ten-year simulation scenario. In our case, if the spills are cleaned up regularly pollution of groundwater represents a small risk within the foreseeable future.

Declaration of Competing Interest

The authors declare that they have no known competing financial interests or personal relationships that could have appeared to influence the work reported in this paper.

Acknowledgments

The authors would like to thank the Cooperative Research Centre for Contamination Assessment and Remediation of the Environment (CRC CARE), BHP Billiton Ltd and the University of Newcastle for making this research possible. This research was funded by CRC CARE Pty Ltd. The research was conducted in the laboratories of the Global Centre for Environmental Remediation (GCER) at the University of Newcastle.

Appendix A. Supplementary data

Supplementary data to this article can be found online at https://doi.org/10.1016/j.geoderma.2019.114017.

References

Ali, S.A., Hagos, H., 2016. Estimation of soil erosion using USLE and GIS in Awassa Catchment, Rift valley, Central Ethiopia. Geoderma Regional 7 (2), 159–166.
Benka-Cooker, M.O., Ekundayo, J.A., 1995. Effects of oil spill on soil physio-chemial properties of a spill site in the Niger delta area of Nigeria. Environ. Monit. Assess. 36, 93–109.
Devatha, C.P., Deshpande, V., Renukaprasad, M.S., 2015. Estimation of soil loss using USLE model for Kulhan watershed, Chattisgarh – a case study. Aquat. Proc. 4 (Suppl. C), 1429–1436.
Ganasri, B.P., Ramesh, H., 2016. Assessment of soil erosion by RUSLE model using remote sensing and GIS – a case study of Nethravathi Basin. Geosci. Front. 7 (6), 953–961.
German, W.L., Harding, D.A., 1969. The adsorption of aliphatic alcohols by montrnorillonite and kaolinite. Clay Miner. 8, 213–227.

Greene-Kelly, R., 1954a. Sorption of aromatic organic compounds by montrnorillonite. Part I. Orientation studies. Trans. Faraday Soc. 51, 412–424.
Greene-Kelly, R., 1954b. Sorption of aromatic organic compounds by montrnorillonite. Part II. Packing studies with pyridine. Trans. Faraday Soc. 51, 425–430.
Head, I.M., Singleton, I., Milner, M.G., 2003. Bioremediation: A Critical Review. Horizon Scientific Press, England.
Karickhoff, S.W., 1981. Emi-empirical estimation of sorption of hydrophobic pollutants on natural sediments and soil. Chemosphere 10, 833–846.
Kassam, A.H., Van Velthuizen, H.T., Mitchell, A.J.B., Fischer, G.W., Shah, M.M., 1992. Agro-Ecological Land Resource Assessment for Agricultural Development Planning.
Kulikov, M., et al., 2017. Modelling soil erodibility in mountain rangelands of South-Western Kyrgyzstan. Pedosphere.
Ma, W., You, X., Wang, X., Chen, Y., 2014. Numerical simulation of migration and transformation of petroleum hydrocarbons in soils. Adv. Mater. Res. 1073–1076, 653–656.
Mercer, J.W., Cohen, R.M., 1990. A review of immiscible fluids in the subsurface. J. Contamin. Hydrol. 6, 7–163.
Miller, W., Miller, D., 1987. A micro pipette method for soil mechanical analysis. Commun. Soil Plant Sci. 18, 1–15.
Mitasova, H., Hofierka, J., Zlocha, M., Iverson, L.R., 1996. Modelling topographic potential for erosion and deposition using GIS. Int. J. Geogr. Inf. Syst. 10, 629–641.
Nathwani, J.S., Philips, C.R., 1997. Adsorption-desorption of selected hydrocarbons in crude oil and soils. Chemosphere 4, 157–162.
Nudelman, N.S., Rios, I.S., Katusich, O., 2002. Fate of the oil residuals in Patagonian soils effects of the environmental exposure time. J. Environ. Assess. Remediat. 3, 1–8.
Olejnik, S., Posner, A.M., Quirk, J.P., 1974. Swelling of montmorillonite in polar organic liquids. Clay Miner. 22, 361–365.
Pan, F., Ma, J., Wang, Y., Zhang, Y., Chen, L., Edmunds, W.M., 2013. Simulation of the migration of transformation of petroleum pollutants in the soils for the Loess plateau: a case study in the Maling oil field of northwestern China. Environ. Monit. Assess. 185, 8023–8034.
Renard, K., et al., 1997. Predicting Soil Erosion by Water: A Guide to Conservation Planning with the Revised Universal Soil Loss Equation (RUSLE). U.S. Department of Agriculture, Agricultural Research Service.
Rogers, J.H., Kennedy, G.M., Davis, S.W., 2002. Comparison of K factors using two different nomographs on surface soils in the Lake Tahoe Basin, California-Nevada. Soil Horizons 43 (2), 53–57.
Römkens, M., Prasad, S., Poesen, J., 1987. Soil Erodibility and Properties.
Sadler, R., Connell, D., 2003. Analytical methods for the determination of total petroleum hydrocarbons in soil. In: Langley, M.G.A., Kennedy, B. (Eds.), The 5th National Workshop on the Assessment of Site Contamination. enHealth, Adelaide SA, Australia.
Simunek, J., Sejna, M., van Genuchten, M.Th., 2008. The HYDRUS-1D Software Package for Simulating the One-Dimensional Movement of Water, Heat, and Multiple Solutes in Variably-Saturated Media. Department of Environmental Sciences, University of California Riverside, Riverside, CA.
Soriano-Disla, J.M., Janik, L.J., Viscarra Rossel, R.A., MacDonald, L.M., McLaughlin, M.J., 2014. The performance of visible, near-, and mid-infrared reflectance spectroscopy for prediction of soil physical, chemical and biological properties. Appl. Spectrosc. Rev. 49, 139–186.
Uzoije, A.P., Agunwamba, J.C., 2011. Physiochemical properties of soil in relation to varying rates of crude oil pollution. J. Environ. Sci. Technol. 4, 313–323.
Van Genuchten, M.T., Nielsen, D.R., 1985. On describing and predicting the hydraulic properties. Ann. Geophys. 3 (5), 615–628.
Wang, L., Yang, D., Fang, C., Chen, Z., Lesniewski, P.J., Mallavarapu, M., Naidu, R., 2015. Novel methodologies for anutomatically and simultaneously determining BTEX components using FTIR spectra. Talanta 144, 1104–1110.
Wang, L., Cheng, Y., Lamb, D., Dharmarajan, R., Chadalavada, S., Naidu, R., 2019. Application of infrared spectrum for rapid classification of dominant petroleum hydrocarbon fractions for contaminated site assessment. Spectrochim. Acta, Part A 207, 183–188.
Williams, S.D., Ladd, D. E., Farmer, J. J., 2003. Fate and Transport of Petroleum Hydrocarbons in Soil and Ground Water at Big South Fork National River and Recreation Area, in Geological Survey Scientific Investigations Report 2005–2014. Tennessee and Kentucky, 2002–2003, U.S. p. 29.
Wischmeier, W.H., Smith, D.D., 1978. Predicting Rainfall Erosion Losses – A Guide to Conservation Planning. USDA, Science and Education Administration, Hyattsville, Maryland, pp. 62.
Yong, R.N., Mohamed, A.M.O., Warkentin, B.P., 1992. Principles of Contaminant Transport in Soils. Elsevier, Amsterdam.